Optimization and Validation of an Artificial Bladder Design Through Finite Element Analysis to Meet Clinical Requirements

Alessio Capecchi, Federica Semproni, *Graduate Student Member, IEEE*, Veronica Iacovacci, *Member, IEEE*, and Arianna Menciassi, *Fellow, IEEE*

***Abstract*—Bladder cancer and urinary dysfunctions present significant challenges to patient health and quality of life. Considering that radical cystectomy remains the standard treatment for muscle-invasive bladder cancer, there is an urgent need for the implantation of artificial bladders (ABs). In this study, we present the optimization and validation of a novel, collapsible, origami-based AB through Finite Element Method (FEM) simulations. We evaluated various materials and wall thicknesses to improve unfolding capability and minimize structural stress concentrations. Simulations were conducted under different filling conditions, replicating the in-body constraints posed by surrounding organs. The optimal material-thickness combination, namely MoldStar 15 with a 2:1 wall-to-fold ratio, effectively maintained low intravesical pressures during filling (0.5-1.96 kPa), meeting the clinical requirements for renal function preservation. Stress analysis showed Von Mises stresses lower than 2.5 MPa, well below the material's tensile stress limit, thus ensuring the structural integrity of the device. The AB model was validated by comparing FEM simulation results with a physical prototype, showing a pressure difference of approximately 15% and a volumetric overlap deviation under 10%.**

***Index Terms*—Soft artificial bladder, bionic artificial organs, design optimization, finite element method (FEM), mechanical simulation.**

I. Introduction

WORLDWIDE, urinary bladder cancer presents an annual incidence of about 573,000 new cases [1]. Muscle-invasive tumors (30% of cases) are generally treated with the surgical removal of the entire bladder and the urethra (radical cystectomy) to avoid recurrence. Following cystectomy, clinical procedures to restore continence include urinary diversion from the kidneys to external collection bags or neobladder reconstruction with autologous tissue [2]. However, these procedures may entail several complications, including the potential onset of infections, and reduction in the patient quality of life. Over the years, researchers explored implantable bioartificial and artificial bladders (ABs) to substitute the native counterpart and to overcome the current limitations of clinical procedures [3]. However, none of these solutions have reached clinics due to implant failure, including the overgrowth of fibrotic tissue, infections, urine leakage from urethral or ureteral anastomoses, and biocompatibility issues [4]. Recently, a novel approach was proposed to make a step forward in the development of efficient ABs. The proposed bioinspired soft and flexible AB is designed as a collapsible structure, derived from an origami-based hexagonal shape [5], [6]. This design allows the AB to occupy a little volume when empty, while assuming an almost spherical shape when full, thus mimicking the native bladder behavior [7]. In addition to continence, the origami-based structure, featuring both flat and foldable surfaces, facilitates the integration with potential actuation and volume-monitoring systems, which are critical for restoring active voiding and proprioception [7]. Moreover, it allows controlled unfolding process as the bladder transitions from empty to full states, minimizing material stretching and thereby reducing the risk of degradation over time. When designing an AB, the use of a biocompatible and soft materials is a key requirement to ensure safe interaction with host tissues once implanted, as well as to maintain low intravesical pressure to preserve renal functions [8]. Meeting all these requirements necessitates careful design and materials selection. As a first step of the designing process, the choice of the geometric and mechanical properties of the AB should be prioritized. In this sense, finite element method (FEM) simulations can support the design, by allowing to explore how different combinations of parameters can affect the operation of the prototype and predict its performance [9].

Over the past decade, medical devices design has vastly benefited from the integration of FEM analyzes in the product development process, typically translating into the verification of device performance in a virtual domain that mirrors its intended real-life application [10]. The advantages of FEM in the medical field lies in a preliminary virtual analysis prior to costly prototyping and bench testing, speeding up the overall process by reducing bench testing iterations and helping in the prediction of long-term device behavior [11], [12], [13]. However, this approach is still not widely utilized in research in the field of artificial organs.

Received 21 January 2025; revised 7 April 2025; accepted 15 May 2025. Date of publication 25 June 2025; date of current version 21 August 2025. This article was recommended for publication by Associate Editor A. Jafari and Editor P. Dario upon evaluation of the reviewers' comments. This work was supported by the Fondo Italiano per la Scienza (FIS), through Innovative Biorobotic Artificial Organs (IBRIS) Project Framework under Grant FIS00001278. *(Corresponding author: Arianna Menciassi.)*

The authors are with the BioRobotics Institute, Scuola SuperioreSant'Anna, 56127 Pisa, Italy (e-mail: arianna.menciassi@santannapisa.it).

This article has supplementary downloadable material available at https://doi.org/10.1109/TMRB.2025.3583192, provided by the authors.

Digital Object Identifier 10.1109/TMRB.2025.3583192

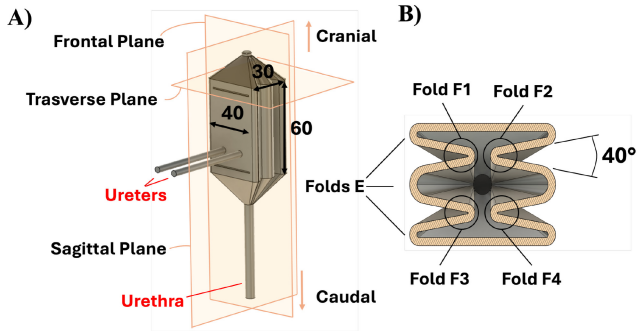

Fig. 1. Representation of A) the AB in anatomical position, with the urethra facing downwards, in which the body planes and directions are shown together with the main AB dimensions expressed in [mm] and B) sectional view of the AB to visualize the walls thickness, the angle between the lateral faces and the nomenclature of internal (F) and external (E) folds.

In this paper, we present a simulation framework to optimize the origami-based AB structure. Our approach focused on refining wall thickness and selecting an appropriate material to enhance the transition between empty and full states, while ensuring gentle contact with surrounding organs to move towards an AB that could function effectively and safely once implanted. To this aim we simulated the filling of the AB under different conditions, while analyzing the intravesical pressure and the deformed geometry. The presented simulations represent a simplified tool for simulating soft devices without the use of CFD, while still reproducing fluid-structure interaction. The paper is organized as follows: Section II presents the design of the proposed AB, detailing the simulation methods with a particular emphasis on the characteristics of the FEM model. Additionally, it outlines the prototype fabrication process and the series of tests performed to validate and assess the optimized model's performance. Section III presents and discusses the results, leading to the selection of the optimal parameters combination. Finally, Section IV provides conclusions drawn from this study.

II. Materials and Methods

A. CAD Modeling of the AB and FEM Analysis Setting

Anatomical knowledge suggests a spherical shape of the human bladder, which can expand to accommodate up to 400-600 mL of urine in adults [14]. The elastic properties and morphology of the bladder tissue allow the maintenance of a low intravesical pressure in the range of 0.9 - 4 kPa to prevent damage to the upper urinary tract during filling [15]. In designing an AB, the primary goal should be the restoration of the urine collection, while ensuring safe integration with the surrounding anatomy, promoting implantation in the abdominal cavity.

Considering these observations, the proposed AB features two inlets and one outlet (Figure 1A) originating from the anatomical positions of the ureters and urethra to facilitate anastomosis with the residual anatomy during implantation [8]. The overall dimensions of the AB correspond to a urinary bladder with a capacity of 200 mL (typical volume of neobladders [16]), achieved through the unfolding mechanism of the lateral AB walls. In this sense, the folds transition from an angle of approximately 40° when the AB is empty (Figure 1B), to 180° when fully filled. The designed folding mechanism facilitates both filling and emptying, by taking also advantage of the spring-back effect.

With the aim of optimizing this AB structure using FEM simulations, the AB was designed in Autodesk Fusion 360 (Autodesk Inc., San Rafael, California, United States), incorporating all design choices to create a 3D model that accurately represents the bladder structure. The AB model was imported into the simulation software Abaqus/CAE (Dassault Systèmes, Vèlizy-Villacoublay, France) to perform filling simulations. The model properties were defined in terms of mesh and load condition. In this sense, linear tetrahedral elements of type C3D4 (size of 0.6 mm) were selected to obtain the mesh. An internal cavity filled with fluid, mimicking the urine in the bladder, was defined using the Fluid Cavity function and the Fluid Cavity Properties (Bulk Modulus and Density set to 1.96 GPa and 1100 kg/m^3, respectively [17]). A frictionless contact property was selected to represent the interaction between the AB walls, minimizing the computational load. As boundary conditions, the AB was fixed in space in all three rotations and translations, with a fixed constraint (6 degrees of freedom) applied to the lower extremity of the urethra as not to hinder the unfolding of the walls. To simulate the filling process, the internal fluid pressure was varied from 0 kPa to a maximum limit of 4 kPa, equivalent to the maximum intravesical pressure identified as reference in humans [15]. The pressure increase was set to occur linearly over time, resulting in a corresponding change in the internal volume. A Dynamic Explicit analysis was conducted with a simulation duration of 1 second, with the minimum increment for the time step set to 10^{-4} seconds.

B. AB Material and Walls Thickness Assessment

Three different materials with varying mechanical properties were simulated, namely Sylgard 184 (DOW), MoldStar 15 (Smooth-on Inc) and Ecoflex 00-30 (Smooth-on Inc). The materials were selected from the silicone family due to their biocompatibility and flexibility, which contribute to low toxicity, softness, and easy manufacturing [18], [19], [20]. Hyperelastic models were utilized for modeling these materials, by assuming silicone rubber as isotropic and incompressible. In order to reduce the computational load, all inelastic phenomena, such as viscoelasticity and stress-softening, were neglected for our purposes, as they do not impact on the bladder deformation. In the simulations, the hyperelastic models rely on the definition of a strain energy function W (or strain energy density), which is the amount of elastically stored energy in a unit volume of material under the state of stretch [21], [22], [23]. Two state of the art hyperelastic models were used in simulation to describe the behavior of the tested materials. Specifically, the Neo-Hookean model was applied to MoldStar 15, while the Ogden model was used for Ecoflex 00-30 and Sylgard 184, as studies in the literature indicate that these models most accurately replicate the behavior of these materials [21]. In these two models, the energy function W can be defined as follows:

$$W_{Ogden} = \sum_{n=1}^{N} \frac{m_n}{a_n}\left({l_1}^{a_n} + {l_2}^{a_n} + {l_3}^{a_n} - 3\right) \quad (1)$$

where N defines the degree of complexity of the model, μ is a deformation resistance coefficient, α is a parameter that controls the nonlinear behavior, and λ represents the principal stretches.

$$\begin{cases} W_{Neo-Hookean} = C_1(I_1 - 3) \\ C_1 = \frac{s}{2} \end{cases} \quad (2)$$

where s is the shear modulus and I is the strain tensor invariant [24]. The parameters used in the Abaqus/CAE software were derived by literature and are shown below. Neo-Hookean model used for MoldStar 15 presents C_1=*0.119* and D_1=*0* [25], [26], while Ogden model for Ecoflex 00-30 is a third-order model with $\mu_1 = 0.001887$, $\alpha_1 = -3.848$, $\mu_2 = 0.02225$, $\alpha_2 = 0.663$, $\mu_3 = 0.003574$, $\alpha_3 = 4.225$, $D_1 = 2.93$ [21] and for Sylgard 184 is a first-order model with $\mu_1 = 0.7637$, $\alpha_1 = 3.5633$, $D_1 = 0.2709$ [27]. To evaluate the impact of folds thicknesses in the AB transition from the empty to the full state, three AB designs were created by changing AB walls thickness (Figure 1B), while keeping a constant internal volume. The ABs behavior was assessed in terms of shape transition predictability with respect to the hexagonal origami sections and the intravesical pressure. Initially, an AB with a constant 2 mm walls and folds thickness was modeled (named *Thickness 2 mm* in this paper). This thickness allows AB lateral walls to bend without significant resistance, while allowing simple and reliable manufacturing through molding. Afterwards, it was decided to uniformly reduce the AB walls thickness down to 1 mm, that is the minimum thickness to achieve a reliable mold through the 3D printer-S300X IDEX, Lynxter (named *Thickness 1 mm* in this paper). As a last case study, only the thickness in the external (E) and internal (F) folds (see Figure 1B) was reduced to 1 mm, by maintaining 2 mm thickness for the flat walls (with a 2:1 wall-to-fold ratio) to investigate whether this anisotropy could facilitate selective unfolding and bending at specific points in the structure (named *Thickness 2-1 mm* in this paper).

C. AB Optimization Using Simulation

AB design optimization refers to the selection of the material- thickness combination able to ensure that the AB (*i*) maintains intravesical pressures in a safe physiological range during filling, (*ii*) results in a deformed geometry similar to the expected shape, (*iii*) does not experience excessive material stress, which could lead to structural damages. All the simulation outputs were compared with reference values, such as the physiological native bladder pressures [15] and the expected hexagonal origami sections. Initially, simulations were conducted varying the AB material and using a 2 mm wall-thickness uniform AB model. After selecting the optimal material among the three tested ones, different AB thicknesses were analyzed. The intravesical pressure was measured at each 25 mL increments whereas the deformed geometry of the AB was extracted at different filling volumes of 100, 150 and 200 mL, analyzed in terms of bladder length (L), width (W), and height (H) and folds opening angles

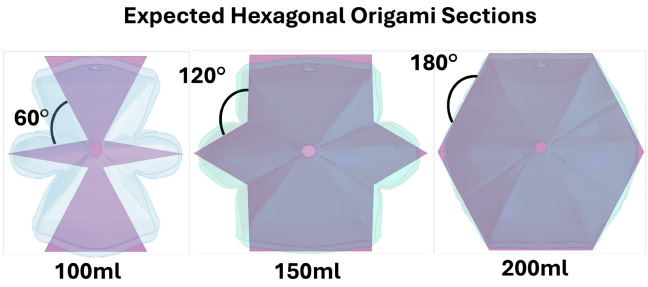

Fig. 2. Representation of the AB expected hexagonal sections (in pink) and folds opening angles for various filling volumes (100, 150, 200 mL), overlaid onto the sections derived from the simulations (in green).

over two transversal planes (i.e., at the cranial and caudal levels, for considering the effect of gravity on urine).The expected hexagonal sections were generated using MATLAB software starting from a parallelepiped with a hexagonal cross-section and performing theoretical calculations of folds deployment (shown in Figure 2). We decided to measure only the angles of internal folds (named F_i in Figure 1B), as they are complementary to the external ones (named E_i in Figure 1B). The comparison of the expected and simulated sectional areas (SA) and folds opening angles (OA), were performed using the following parameters:

$$SA\% = \frac{Expected\ Section}{Simulated\ Section} \times 100 \quad (3)$$

$$OA\% = \frac{Expected\ Angle}{Simulated\ Angle} \times 100 \quad (4)$$

The simulations were analyzed also in terms of stresses experienced by the AB during the filling cycles, to ensure that no areas and folds exceed the tensile strength limit specific to each material (6.7 MPa for Sylgard 184, 2.8 MPa for MoldStar 15, and 1.4 MPa for Ecoflex 00-30) [28]. Once defined the optimal combination of AB material-thickness, two additional simulations were performed to reproduce a more realistic operative scenario, thus, to evaluate the AB behavior when positioned in the abdominal cavity. We considered: (*i*) positioning the AB model with the urethra facing downward and applying the effect of gravity to simulate a standing patient, and (*ii*) adding surrounding obstacles (in different positions) to simulate the presence of the abdominal organs around the bladder. For simplicity, the obstacles were modeled as spheres with different sizes of 80 mm and 20 mm diameter, similar to the size of the stomach and small intestine [29], [30]. To reduce the computational load, the spheres were considered as discrete rigid and fixed bodies around the AB to hinter its opening during filling. In both cases, the AB urethra was anchored with a fixed constraint to simulate the surgical anchoring to the residual anatomy. The results of the simulations were assessed during filling cycles, employing the same output parameters previously described.

D. Validation of the Simulated Model Using an AB Prototype

A validation of the simulations was performed to ensure that the computational model of the AB accurately represented real-world behavior during filling cycles. This validation is

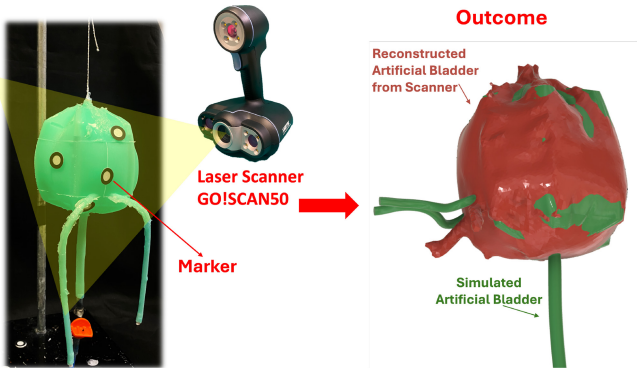

Fig. 3. Representation of the experimental setup for the validation of the artificial bladder simulation under the presence of gravity. The setup includes the AB prototype filled with water, a laser scanner and passive markers attached on the bladder walls.

crucial to define whether the model could reliably predict the AB performance and functionality in practical applications. For this purpose, an AB prototype with the optimal material-thickness combination was fabricated using the injection molding technique, typically employed for prototyping soft structures. The AB mold was designed with Autodesk Fusion 360, 3D printed using FDM 3D printer (Original Prusa i3 MK3s+3D printer) and subsequently used for silicone injection. The AB was tested during filling cycles under two conditions: (i) positioned with the urethra facing downward to simulate the patient standing posture, subjected only to gravitational force, and (ii) placed inside a human mannequin replicating the abdominal cavity with the addition of water-filled balloons (sizes of 40-80 mm diameter) simulating the presence of surrounding organs. An inextensible tape was used to restrict the movement of the water-filled balloons, mimicking the presence of the abdominal wall (see Supplementary Video S2). The AB filling was performed using a syringe, with the fluid introduced through the urethra. One ureter was kept collapsed to prevent fluid leakage, while the other was connected to a pressure sensor (MPX5100DP series; Freescale Semiconductor, Inc.). The AB was gradually filled up to a capacity of 200 mL, intravesical pressure values were recorded at every 25 mL of increase in volume. For the first test, passive markers were placed on the prototype to allow the reconstruction of the AB outer surface through a laser scanner (GO!SCAN50, Creaform Inc.) with the aim of analyzing the geometry of the prototype. Scans were performed at 100 mL, 150 mL, and 200 mL of filling volumes (Figure 3). For each scan, a mesh refinement was first performed using MeshLab software to cancel imaging holes and eliminate unnecessary surfaces resulting from the scanning. Then, the mesh was imported into Fusion360, allowing us to obtain two sections for each scan, one cranial and one caudal respect to the anatomical location of the bladder (see Figure 1A). For the second test involving the presence of water-filled balloons, no scans were performed due to the lack of a direct line of sight caused by the presence of the mannequin and the positioning constraints. The experimental results were compared with the simulation conducted under realistic conditions, both when applying the effect of gravity force (pressure and volume) and when simulating the presence of surrounding organs (pressure only).

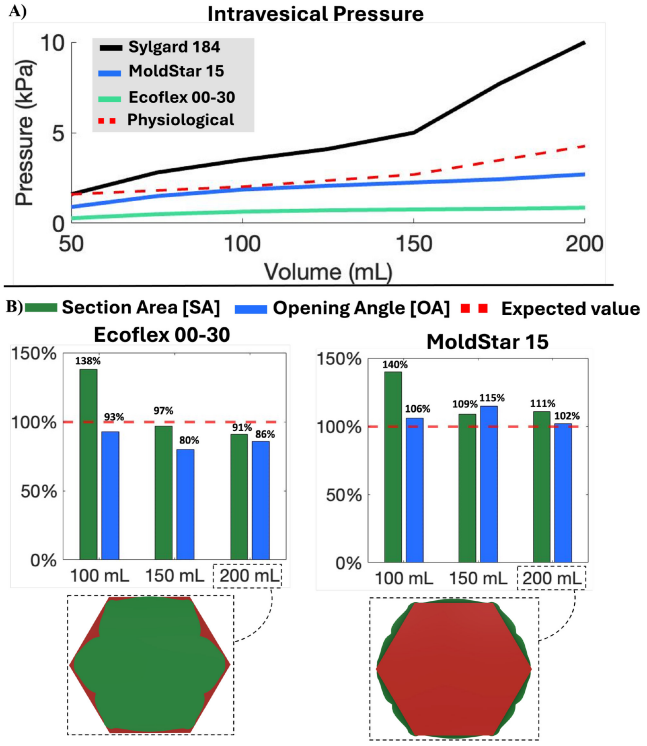

Fig. 4. A) Representation of the intravesical pressures as a function of the filling volumes, for the simulations performed for three different silicone materials Sylgard 184 (in black), MoldStar 15 (in blue) and Ecoflex 00-30 (in green), compared to the physiological pressures of the native urinary bladder (in red). B) Representation of the SA and OA (Equation 3, 4) results for Ecoflex 00-30 and MoldStar 15 ABs, with a focus on the comparison of the median cross-sections between the simulations (green) and the expected hexagonal shape (red)

III. Results and Discussion

A. Choice of the AB Material

The first analysis conducted in this work involved the testing of various AB materials (maintaining walls thickness of 2 mm), while monitoring the intravesical pressure and the geometrical parameters during the filling simulation. As shown in Figure 4A, the intravesical pressures exceeded the physiological limit (in red) when considering an AB made of Sylgard 184 (in black). This depends on the stiffness of the material, which require high force to expand the AB walls. MoldStar 15 (in blue) and Ecoflex 00-30 (in green) allowed the internal pressures to remain below the physiological threshold, ensuring safe operation during filling cycles. Considering the Von Mises stresses, the tensile strength limit was exceeded in the case of Sylgard 184, reaching values up to 11 MPa. In contrast, none of the other two materials exceeded their tensile stress limit, with maximum stress values of 0.85 MPa for Ecoflex 00-30, and 2.6 MPa for MoldStar 15. These observations lead to discard Sylgard 184, indicating a potential risk for renal function and for damaging the silicone structure itself. Geometrical considerations, in terms of SA and OA parameters, were carried out for the two remaining materials.

As shown in Figure 4B, SA values (green bars) do not exhibit significant differences between the two materials, with values slightly below the reference for Ecoflex 00-30 and above the reference for MoldStar 15, for volumes of 150 mL and 200 mL. Slightly higher difference is observed for OA values (blue bars), with values around 80% for Ecoflex 00-30 and 105% for MoldStar15. The tendency of Ecoflex 00-30 to unfold less, still managing to contain the entire fluid, resulted in a deformation along the cranial-caudal axis, with an increasing length L of 30% (while 15% was observed for MoldStar 15). In view of a potential sensing application, this reduced unfolding could lead to inaccurate estimation of the actual internal volume, potentially creating a risk when managing voiding [5]. By combining the various results, Ecoflex 00-30 was discarded and the following simulations aimed at shedding the light on AB behavior with different walls thicknesses were performed by considering AB made of MoldStar15.

B. Choice of Wall Thicknesses

Once selected the material that allowed to closely achieve the expected hexagonal shape (i.e., Moldstar15), the mechanical and geometrical analysis was repeated varying the AB walls thicknesses (i.e., *Thickness 2 mm*, *Thickness 1 mm* and *Thickness 2-1*). For all the three wall thicknesses, the AB intravesical pressures remained below the physiological range during filling, as shown in Figure 5A. While the thicker walls case (i.e., *Thickness 2 mm*) allows for a more robust structure, it also results in larger pressures, i.e., about 1 kPa higher than *Thickness 1 mm*. In terms of Von Mises stresses, none of the ABs exceed the tensile strength limit of 2.8 MPa, with maximum stress values of 2.6 MPa for *Thickness 2 mm* and *Thickness 1 mm*, and 2.3 MPa for *Thickness 2-1 mm*. However, analysis of the stress distribution on the AB structures revealed that the *Thickness 2 mm* reached stress levels around 2 MPa along the internal folds (F in Figure 1B), whereas *Thicknesses 1 mm* and *Thickness 2-1 mm* only reached stress levels of about 0.5 MPa. From these considerations, it has emerged that having thinner thickness in the folds (*Thickness 2-1 mm* case) facilitates unfolding, while also allowing limited stresses on the overall AB structure. Analyzing the geometrical deformations of the ABs, the *Thickness 1 mm* case showed greater deviations from the expected behavior, with SA values around 90% (green bars Figure 5B) and OA values around 70% (blue bars in Figure 5B). In contrast, the other two cases do not show significant deviations from the expected geometry, with maximum deviations of around 10% and 2%, respectively.

Also in these cases, deviations from the reference values resulted in a protrusion of the overall structure, with an H deviation of 7.5% for *Thickness 1 mm* (6% for *Thickness 2mm*, and 3% for *Thickness 2-1 mm*). Based on the obtained results, *Thickness 2-1 mm* AB demonstrated closer alignment with theoretical reference values, leading to its selection for the final design. Figure 6 shows the stresses to which the final AB design in MoldStar15 with *Thickness 2-1 mm* is subjected. The internal folds (F) experienced higher stress, reaching values of around 0.5 MPa, compared to the external folds (E), which

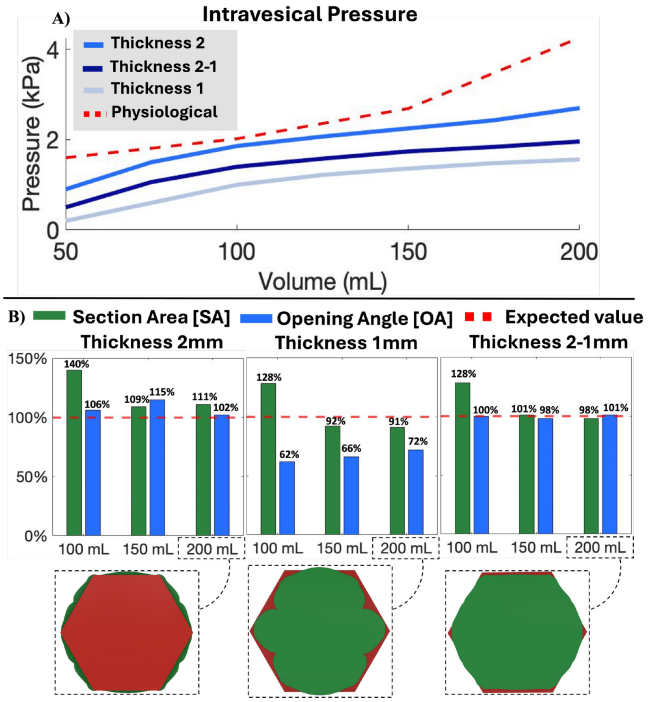

Fig. 5. A) Representation of the intravesical pressure as a function of the filling volume for the simulations performed with AB made of MoldStar15 with different thicknesses. The physiological pressure range is shown in black to allow comparison; B) Representation of the SA and OA (Equation 3, 4) results and the comparison of the cross-sections between the simulations (in green) and the expected hexagonal shape (in red), in the case of simulations performed on AB made of MoldStar 15 with different thickness: *Thickness 2 mm*, *Thickness 1 mm*, and *Thickness 2-1 mm*, for filling volumes of 100, 150 and 200 mL.

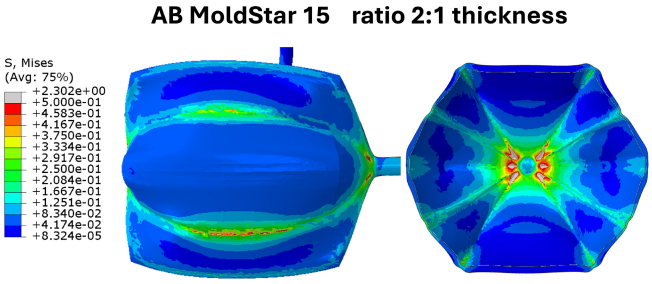

Fig. 6. Representation through a side view and a sectional view in the transverse plane of the stress trend, obtained from the simulation of AB *Thickness 2-1 mm* in MoldStar15.

reached values around 0.3 MPa. This difference is due to the larger opening range (up to 180°) experienced during filling by the internal folds, compared to the external ones (opening angles up to 120°). There are areas of higher stress concentration, along the junctions of the inner folds on the caudal face (Figure 6), reaching values of 2.3 MPa, which is anyhow below the Tensile Strength limit of MoldStar 15. This ensures the structural integrity of the AB and demonstrates the safety of the overall AB structure. As a final step, the behavior of the optimized AB when positioned in the abdominal cavity was simulated by adding surrounding obstacles. As expected, the presence of obstacles that hinter the AB unfolding lead to an increase in pressure (dotted lines in Figure 7). Specifically, in the cases with 1 and 2 obstacles, the AB experiences an increase of about 0.1 kPa. Adding more obstacles (4

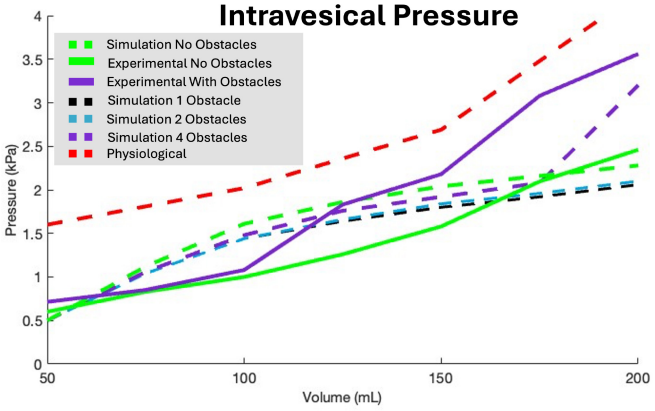

Fig. 7. Representation of the intravesical pressure as a function of the filling volume, derived from AB simulations (dotted lines) with *Thickness 2-1 mm* in MoldStar15 without obstacles (in green), with obstacles (in black, light blue and purple), and extracted from experimental testing (solid lines) without obstacles (in green), with obstacles (in purple). Physiological pressure (in dotted red line) is also included for comparison.

obstacles) does not lead to a significant pressure increase for filling volume below 175 mL. Beyond this point, the pressure abruptly increased reaching a peak of around 3.2 kPa. The presence of obstacles surrounding the AB induces spatial redistribution during the filling process; as the number of obstacles restricting spatial movement increases, the resultant pressure rise becomes more pronounced. However, the values always stay below the physiological limit of approximately 4 kPa, guarantying safety for the upper urinary tract structures. Even though the obstacles hinter bladder opening (maximum opening angles around 130° rather than 180°), the AB managed to reach a filling volume of 200 mL without excessively stressing the material, remaining below the MoldStar 15 tensile strength limit. Noteworthily, the approximation of organs simulated as rigid bodies allowed us to evaluate the pressure and stresses behavior in a worst-case scenario. In fact, we would expect lower values of both pressure and stresses in case of implantation in the abdomen where all surrounding organs are soft (see Supplementary Video S1).

C. Validation Results

Simulations validation was carried out by comparing the behavior of the simulated AB (in MoldStar 15 and *Thickness 2-1 mm*) with a physical prototype during filling cycles. Experimental intravesical pressure features a trend comparable to the simulated AB when subjected to the gravitational force (green lines in Figure 7) with pressure increasing gradually during filling (maximum difference of 0.18 kPa at 200 mL) but still below the physiological limit. In the presence of obstacles mimicking the surrounding organs, both simulation and experimental tests indicate an increase of approximately 1 kPa (purple lines in Figure 7) compared to the unobstructed scenario (green lines in Figure 7). This confirms the AB capacity to hold 200 mL of fluid while keeping intravesical pressure below the physiological limit. In all tested scenario, the discrepancy between simulation and experimental results remains around 15%, in line with literature value [31]. It is evident that the intravesical pressure in the case with and without obstacles, both in simulation and in the experimental setup, shows the same trend, thus further validating the reliability of our simulations. This difference can be ascribed both to the approximations and assumption made in the simulated environment, such as absence of friction between AB faces, as well as potential defects in the prototype, like non uniform wall thickness. In terms of SA and OA parameters, we compared the cranial and caudal sectional area and opening angles folds between the simulation (with gravity) and the laser scanned AB. As expected, the application of gravitational load led to an asymmetrical opening of the folds respect to the transverse plane as the fluid tends to concentrate in the caudal section, visible both in the simulation and in the prototype. Figure 8A shows the errors resulting from the comparison between the simulation and experimental tests (calculated as the difference divided by the expected value Figure 2). For both the caudal and cranial sections, the mean error tends to decrease during filling, reaching 10% at AB capacity. Assuming a homogeneous error distribution throughout the AB structure, we express the error in volumetric terms, noting that the maximum discrepancy reaches 20 mL at full capacity (thus 10% of 200 mL). For lower filling volumes (below 150 mL), an increase in error is observed. These errors result from the interplay of multiple factors. Manual identification of sections and angle measurements are particularly vulnerable to human errors. Additionally, the scanner faces difficulty detecting fold angles when they are not fully open, and subsequent mesh processing can further distort the original geometry. When comparing the results between the caudal and cranial sections, the caudal section shows greater errors. This is mainly attributed to fluid accumulation driven by gravity, which deforms the material in the thinner regions caused by the manufacturing process. A similar issue is observed in relation to the sagittal plane, where the simulations exhibit symmetry in the opening of the folds (light blue areas in Figure 8B). However, folds F3 and F4 deviate from this symmetry in the prototype (pink areas in Figure 8B), leading to an increase in SA errors as the volume increases. Despite the errors in predicting the unfolding angles, the overall volumes show good alignment. In fact, by analyzing the cross-section areas (Figure 8C) the simulation accurately predicts the shape of the bladder, with a mean error of 13% and 6% for the caudal and cranial sections, respectively.

IV. Conclusion

The application of FEM simulations in the design and optimization of soft medical devices has transformed the designing process of innovative biomedical technologies. In fact, simulations allow for the evaluation of different geometrical parameters, while reducing both testing time and costs. This is particularly true when considering implantable devices, where simulations provide a high-fidelity replication of the physiological environment, reducing also the need for in-vivo testing. This paper focuses on using FEM simulations to optimize an origami-based hexagonal AB [5], designed for implantation in the abdominal cavity as a replacement for the native bladder in patients who have undergone radical

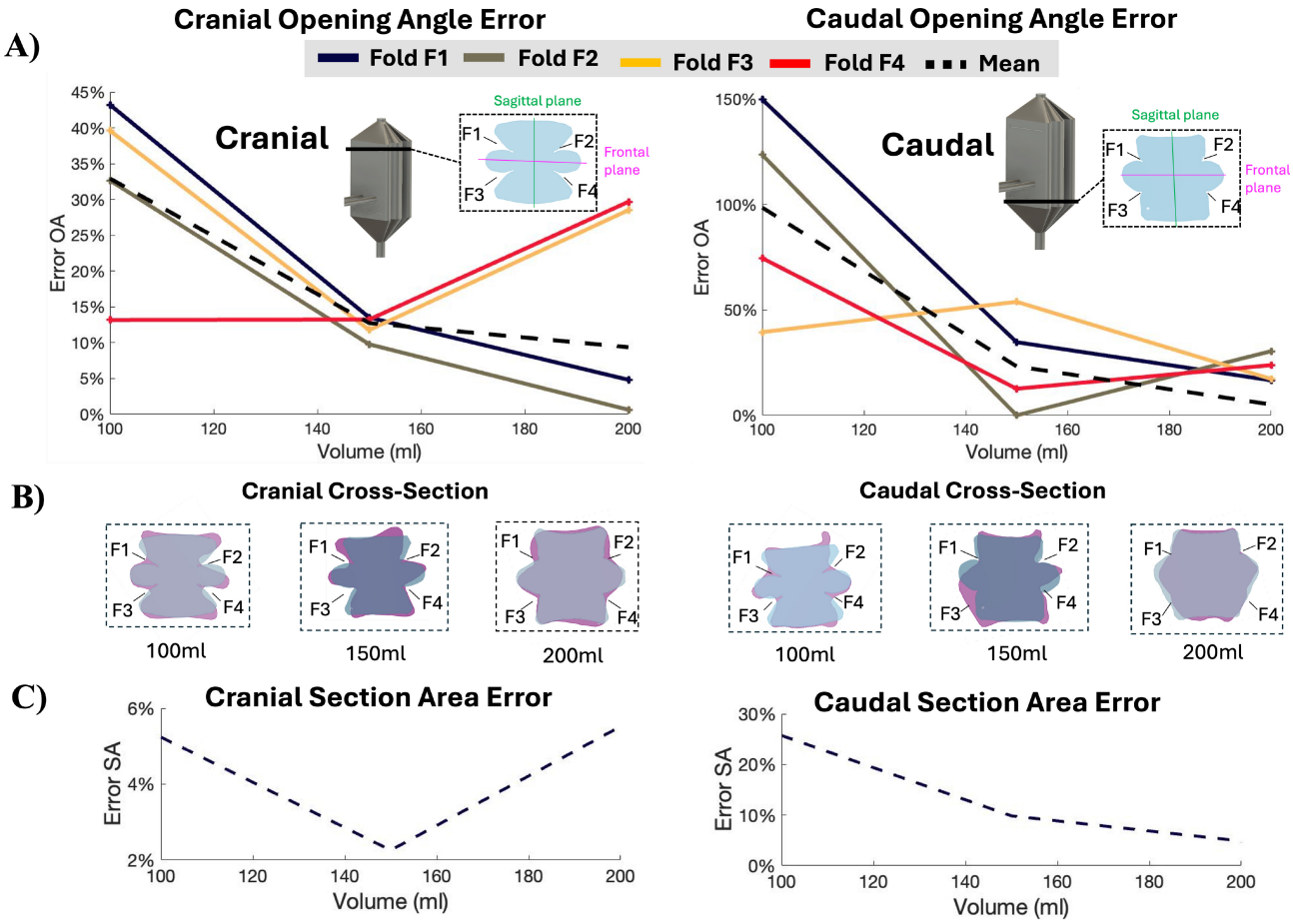

Fig. 8. A) Representation, for the cranial and caudal cross-section, of the fold opening angles error between the prototype and simulation measured in the internal folds, defined as F1, F2, F3, and F4; B) Representation of the overlapping cross-sections of cranial and caudal regions obtained from simulations (light blue) and the prototype (light purple); C) Representation, for the cranial and caudal cross-section, of the section area error between the prototype and simulation. All results are measured for the internal volumes of 100, 150, and 200 mL

cystectomy. The simulations conducted on the proposed AB include the analysis of structural parameters (e.g., material and walls thickness) while monitoring intravesical pressure, geometrical parameters and Von Mises stress. Among the various combinations tested, the AB in MoldStar 15 with thinner folds (*Thickness 2-1*) allowed to assume the desired bladder shape in both empty and filled configurations, facilitating controlled folding of AB origami. This AB showed better performances, maintaining a maximum intravesical pressure of 1.96 kPa, in line with the clinical requirement for preserving renal function, and value of SA and OA deviating from the expected values only by around 2%. The simulations performed reproducing the abdominal cavity demonstrated that the AB functions correctly even in the presence of objects that impede its full opening during filling. Also in this case, the intravesical pressures remained below the physiological limit (maximum of 3.2 kPa), demonstrating its safety in the interaction with the other structures. The optimized AB was validated by comparing the simulation with a physical prototype manufactured by injection molding technique (urethra facing downwards and applying gravity, and AB positioned in a human mannequin with water-filled balloons to mimic surrounding organs). No remarkable differences were observed in terms of intravesical pressure differing by only 15% in both tests, with a maximum pressure during the obstacle test that remains below the physiological limit. The geometrical parameters showed a decreasing trend as volume increases, with an error around 10% and 5% when completely filled, respectively for opening angles of folds and section area in a gravity test.

In this work, we have demonstrated the reliability of our model in representing artificial bladder behavior during filling, achieving results that are comparable to the experimental testing, also in realistic operational conditions. This model serves as the foundation for further analysis of the proposed AB, including its integration with other artificial structures (e.g., actuators for active voiding, urethral and ureteral sphincters), the selection and investigation of long-term certified biocompatible implantable materials with mechanical properties comparable to those of this study, as well as simulating its behavior during the emptying phase. Moreover, cyclic simulations should be performed to evaluate the structural integrity over repeated filling-emptying cycles in simulated in body environment (i.e., temperature and humidity) and to assess the long-term functionality of the AB. However, the use of FEM in designing soft medical devices still presents several open challenges and limitations. First is the complexity of modeling materials properties (viscoelasticity, stress-softening,

incompressibility) and complex soft structures, forcing to use simplifications that partially alter the results compared to reality. Moreover, the Abaqus CAE software enabled a detailed analysis of the structural deformation resulting from fluid–structure interaction, without explicitly modeling the fluid behavior. Furthermore, the focus limited on the static analysis that overlook the impact of dynamic factors on structural integrity, represents an additional key limitation in the simulations, that prevents the assessment of material durability over time, making the transition to prototype testing indispensable. To assess how the structure affects fluid movement, Computational Fluid Dynamics (CFD) simulations or alternative software would be needed. This would enable a focus on fluid dynamics, including flow velocity and stagnation zones, which could impact the AB function and structural integrity. In this sense, surface properties, such as roughness and defects, play a significant role in encrustation, making necessary the use of antifouling or bactericidal coatings [32].

Although prototyping will still be required, FEM has enabled us to accelerate the design and optimization process, replicating and predicting performance under realistic conditions. While this study focused on a specific implementation tailored to our artificial bladder design, the developed simulation framework could be extended to other implantable soft robotic systems and allow geometry and material optimization. For example, soft actuators for native bladder support could benefit from this approach. Notably, this framework simulates the filling of a hollow "reservoir" without the use of CFD, enabling faster yet accurate simulations. The fidelity of the simulation was validated by comparison with a physical prototype, demonstrating that the model reliably captures key deformation and pressure characteristics relevant for design optimization.

ACKNOWLEDGMENT

All authors declare that they have no conflict of interest.

REFERENCES

[1] A. Lopez-Beltran, M. S. Cookson, B. J. Guercio, and L. Cheng, "Advances in diagnosis and treatment of bladder cancer," *BMJ*, vol. 12, Feb. 2024, Art. no. e076743, doi: 10.1136/bmj-2023-076743.

[2] R. Stein, M. Hohenfellner, S. Pahernik, S. Roth, J. W. Thüroff, and H. Rübben, "Urinary diversion," *Deutsches Ärzteblatt Int.*, vol. 109, pp. 617–622, Sep. 2012, doi: 10.3238/arztebl.2012.0617.

[3] D. Rohrma, D. Albrecht, J. Hannappel, R. Gerlach, G. Schwarzkopp, and W. Lutzeyer, "Alloplastic replacement of the urinary bladder," *J. Urol.*, vol. 156, pp. 2094–2097, Dec. 1996.

[4] M. Cosentino, J. M. Gaya, A. Breda, J. Palou, and H. Villavicencio, "Alloplastic bladder substitution: Are we making progress?" *Int. Urol. Nephrol.*, vol. 44, no. 5, pp. 1295–1303, Oct. 2012, doi: 10.1007/s11255-012-0249-2.

[5] F. Semproni, V. Iacovacci, S. Maglio, S. Onorati, M. Ibrahimi, and A. Menciassi, "Soft artificial bladder with volume monitoring capabilities," in *Proc. 15th Hamlyn Symp. Med. Robot.*, London, U.K., Jun. 2023, pp. 93–94, doi: 10.31256/HSMR2023.47.

[6] G. Casagrande, M. Ibrahimi, F. Semproni, V. Iacovacci, and A. Menciassi, "Hydraulic detrusor for artificial bladder active voiding," *Soft Robot.*, vol. 10, no. 2, pp. 269–279, Apr. 2023, doi: 10.1089/soro.2021.0140.

[7] A. K. Patel and C. R. Chappel, "Anatomy of the lower urinary tract," *Renal Urol.*, vol. 26, pp. 127–132, Apr. 2008.

[8] V. Mahadevan, "Anatomy of the lower urinary tract," *Surgery*, vol. 34, no. 7, pp. 318–325, Jul. 2016, doi: 10.1016/j.mpsur.2016.04.001.

[9] D. Zrinscak et al., "Design of a soft robotic artificial cardiac wall," *Artif. Organs*, to be published, doi: 10.1111/aor.14978.

[10] M. Driscoll, "The impact of the finite element method on medical device design," *J. Med. Biol. Eng.*, vol. 39, no. 2, pp. 171–172, Apr. 2019, doi: 10.1007/s40846-018-0428-4.

[11] A. N. Natali, C. G. Fontanella, and E. L. Carniel, "Biomechanical analysis of the interaction phenomena between artificial urinary sphincter and urethral duct," *Numer. Methods Biomed. Eng.*, vol. 36, no. 3, Mar. 2020, Art. no. e3308, doi: 10.1002/cnm.3308.

[12] E. T. Roche et al., "Soft robotic sleeve supports heart function," *Sci. Transl. Med.*, vol. 9, no. 373, Jan. 2017, Art. no. eaaf3925, doi: 10.1126/scitranslmed.aaf3925.

[13] M. Singh et al., "Hemodynamic evaluation of biomaterial-based surgery for Tetralogy of Fallot using a biorobotic heart, in silico, and ovine models," *Sci. Transl. Med.*, vol. 16, no. 755, Jul. 2024, Art. no. eadk2936, doi: 10.1126/scitranslmed.adk2936.

[14] Y. Aoki, H. W. Brown, L. Brubaker, J. N. Cornu, J. O. Daly, and R. Cartwright, "Urinary incontinence in women," *Nat. Rev. Dis. Primers*, vol. 3, no. 1, Jul. 2017, Art. no. 17042, doi: 10.1038/nrdp.2017.42.

[15] R. T. Kershen, K. M. Azadzoi, and M. B. Siroky, "Blood flow, pressure and compliance in the male human bladder," *J. Urol.*, vol. 168, pp. 121–125, Jul. 2002.

[16] B. Barone et al., "Advances in urinary diversion: From cutaneous ureterostomy to orthotopic neobladder reconstruction—A comprehensive review," *J. Pers. Med.*, vol. 14, no. 4, p. 392, Apr. 2024, doi: 10.3390/jpm14040392.

[17] X. Yuan, W. Wang, X. Zhu, and L. Zhang, "Theoretical model of dynamic bulk modulus for aerated hydraulic fluid," *Chin. J. Mech. Eng.*, vol. 35, no. 1, p. 121, Dec. 2022, doi: 10.1186/s10033-022-00794-1.

[18] V. B. Sardar, D. N. R. Rajhans, A. Pathak, and T. Prabhu, "Developments in silicone material for biomedical applications- A review," in *Proc. 14th Int. Conf. Humaniz. Work Work Environ.*, vol. 14, 2016, pp. 1–18.

[19] I. Miranda et al., "Properties and applications of PDMS for biomedical engineering: A review," *J. Funct. Biomater.*, vol. 13, no. 1, p. 2, Dec. 2021, doi: 10.3390/jfb13010002.

[20] Z. Liao, M. Hossain, X. Yao, R. Navaratne, and G. Chagnon, "A comprehensive thermo-viscoelastic experimental investigation of Ecoflex polymer," *Polymer Test.*, vol. 86, Jun. 2020, Art. no. 106478, doi: 10.1016/j.polymertesting.2020.106478.

[21] M. S. Xavier, A. J. Fleming, and Y. K. Yong, "Finite element modeling of soft fluidic actuators: Overview and recent developments," *Adv. Intell. Syst.*, vol. 3, no. 2, Feb. 2021, Art. no. 2000187, doi: 10.1002/aisy.202000187.

[22] R. W. Ogden, *Non-Linear Elastic Deformations*. North Chelmsford, MA, USA: Courier Corp., 1997.

[23] G. A. Holzapfel, *Nonlinear Solid Mechanics: A Continuum Approach for Engineering*. Hoboken, NJ, USA: Wiley, 2000.

[24] S. N. A. M. Noor and J. Mahmud, "Modelling and computation of silicone rubber deformation adapting Neo-Hookean constitutive equation," in *Proc. 5th Int. Conf. Commun. Syst. Netw. Technol.*, Apr. 2015, pp. 1323–1326, doi: 10.1109/CSNT.2015.276.

[25] Y. Hao et al., "A multimodal, enveloping soft gripper: Shape conformation, bioinspired adhesion, and expansion-driven suction," *IEEE Trans. Robot.*, vol. 37, no. 2, pp. 350–362, Apr. 2021, doi: 10.1109/TRO.2020.3021427.

[26] N. Kidambi, R. L. Harne, and K.-W. Wang, "Modular and programmable material systems drawing from the architecture of skeletal muscle," *Phys. Rev. E*, vol. 98, no. 4, Oct. 2018, Art. no. 43001, doi: 10.1103/PhysRevE.98.043001.

[27] L. Pini and F. V. Briatico, "Geometry optimization for biaxial testing of polydimethylsiloxane SYLGARD® 184 and finite element modelling," M.S. thesis, Mater. Eng. Nanotechnol., Politecnico di Milano, Milan, Italy, 2018.

[28] G. Miron and J.-S. Plante, "Design principles for improved fatigue life of high-strain pneumatic artificial muscles," *Soft Robot.*, vol. 3, no. 4, pp. 177–185, Dec. 2016, doi: 10.1089/soro.2016.0011.

[29] G. Hounnou, C. Destrieux, J. Desme, P. Bertrand, and S. Velut, "Anatomical study of the length of the human intestine," *Surg. Radiol. Anat.*, vol. 24, pp. 290–294, Dec. 2022.

[30] E.-G. Lee et al., "Anthropometric study of the stomach," *J. Gastric Cancer*, vol. 16, no. 4, p. 247, 2016, doi: 10.5230/jgc.2016.16.4.247.

[31] J. Zimmermann et al., "Quantitative hemodynamics in aortic dissection: Comparing in vitro MRI with FSI simulation in a compliant model," in *Proc. Funct. Imag. Model. Heart, 11th Int. Conf.*, 2021, pp. 575–586. doi: 10.1007/978-3-030-78710-3_55.

[32] A. Cardona, V. Iacovacci, T. Mazzocchi, A. Menciassi, and L. Ricotti, "Novel nanostructured coating on PDMS substrates featuring high resistance to urine," *ACS Appl. Bio Mater.*, vol. 2, no. 1, pp. 255–265, Jan. 2019, doi: 10.1021/acsabm.8b00586.